Magnetic x-ray investigation at the $L_{2,3}$ edges of Nd in $Nd_2Fe_{14}B$

F. Bartolomé, J. M. Tonnerre, L. Sève, D. Raoux, and J. E. Lorenzo
Laboratoire de Cristallographie, CNRS. BP 166 38042 Grenoble Cedex 9, France

J. Chaboy, L. M. García, and J. Bartolomé
ICMA, CSIC-Universidad de Zaragoza, Facultad de Ciencias, 50009 Zaragoza, Spain

M. Krisch and A. Rogalev
European Synchrotron Radiation Facility, B.P. 220, 38043 Grenoble Cedex, France

R. Serimaa
Physics Department, University of Helsinki, Finland

C-C. Kao
National Synchrotron Light Source, Brookhaven National Laboratory, Upton, New York 11973

G. Cibin and A. Marcelli
LNF, INFN, Frascati, Italy

A systematic study of x-ray magnetic circular dichroism, x-ray resonant magnetic scattering, and resonant inelastic x-ray scattering at the $L_{2,3}$ edges of Nd on $Nd_2Fe_{14}B$ is presented. The combined information allows to assign a dipolar or quadrupolar origin to different features appearing in the experimental spectra and to study the thermal dependence of the Nd moment orientation below the spin reorientation transition which takes place at $T_{SRT}=135$ K. © *1998 American Institute of Physics.* [S0021-8979(98)25011-0]

The possibility offered by near-edge x-ray magnetic techniques of separately probing a given element in a material containing several magnetic species can be used to disentangle a wide set of problems on the magnetism of materials, as, for example, rare-earth (R)-transition metal (TM) intermetallics. However, the interpretation of x-ray magnetic circular dichroism (XMCD) and resonant magnetic scattering (XRMS) at the $L_{2,3}$ edges of R ions ($2p\rightarrow 5d$ transitions) has been a controversial subject since the first experimental results were obtained. It has been pointed out that, to properly describe the observed signals, several aspects had to be included in the analysis, among others the contribution from $2p\rightarrow 4f$ quadrupolar excitation channels in the pre-edge region.[1] In this article, we report on a combined study of XMCD, XRMS, and resonant inelastic x-ray scattering (RIXS) which allows to assign a multipolar origin to the different features appearing in the experimental spectra at the Nd $L_{2,3}$ edges, and to apply this information to the study of the thermal dependence of the orientation of the Nd magnetic moments upon the spin reorientation transition (SRT) taking place on $Nd_2Fe_{14}B$. Below $T_{SRT}\approx 135$ K, the easy axis magnetization direction (EMD) continuously rotates from the [001] axes (high-T phase) towards the [110] axis. Although the behavior of the bulk magnetization has been well determined, the evolution of the magnetic moments on the microscopic scale is less understood. It has been proposed that the Nd and Fe moments can be considerably noncollinear in the low-temperature phase.[2,3] Different macro- and microscopic techniques have been applied to study the SRT, but no general agreement on the mutual orientation of the R and Fe moments in the low temperature phase has been reached so far.[4]

To directly study the reorientation angles of Nd atoms on the SRT, we measured temperature-dependent XMCD at the $L_{2,3}$ edges of Nd in a single crystal of $Nd_2Fe_{14}B$. The chosen geometry was as follows: the incident photon wave vector, $\mathbf{k}_i$, the [001] and the [110] axes of the plate-shaped single crystal lied in the horizontal plane, both [001] and [110] axes forming an angle of 45° with $\mathbf{k}_i$. A magnetic field of 1 T was applied parallel to $\mathbf{k}_i$. In the dipolar approximation ($2p\rightarrow 5d$ transitions), XMCD is proportional to $\cos(\alpha)$, where α is the angle between the Nd atomic magnetic moment, $\overline{\mu}_{Nd}$, and $\mathbf{k}_i$. Below T_{SRT}, $\overline{\mu}_{Nd}$ rotates from the [001] axes by an angle $\theta_{Nd}(T)$. Consequently, the described XMCD experiment is sensible to both, $\theta_{Nd}(T)$ (through $\alpha(T)=45°-\theta_{Nd}(T)$) and $\mu_{Nd}(T)$.

Figure 1 shows five representative XMCD spectra at the $L_{2,3}$ edges of Nd in $Nd_2Fe_{14}B$ recorded at different temperatures in the vicinity of SRT, as indicated in the figure. Two

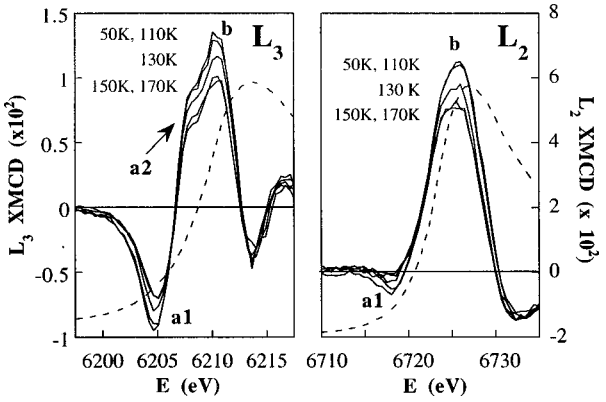

FIG. 1. Normalized XMCD spectra recorded at different temperatures at the L_3 (left panel) and L_2 (right panel) edges of Nd in $Nd_2Fe_{14}B$. The spin averaged absorption ($T=150$ K) is also shown (a.u., dashed line).

a)Electronic mail: bartolom@polycnrs-gre.fr

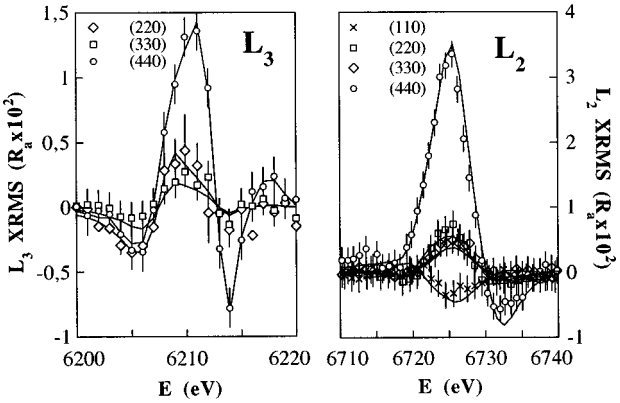

FIG. 2. XRMS asymmetry ratios for several $(hh0)$ Bragg reflections at the L_3 (left panel) and L_2 (right panel) absorption edges of Nd in $Nd_2Fe_{14}B$. Lines are the results of a regularisation analysis fitting including a quadrupolar origin for a1 and a2 features (see Fig. 1).

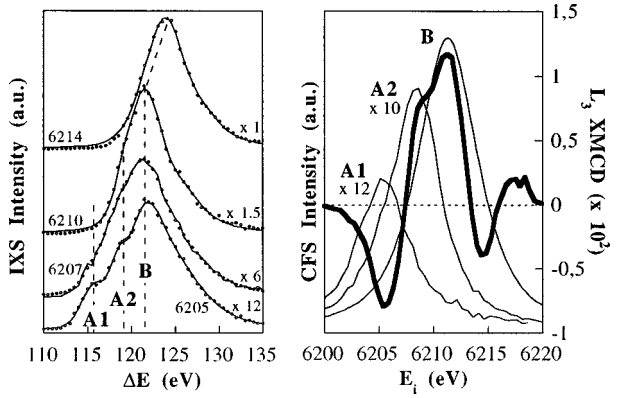

FIG. 3. RIXS intensity at four incident energies (left panel) and CFS scans (right panel, thin lines) together with XMCD (thick line) at Nd L_3 edge on $Nd_2Fe_{14}B$. RIXS data are scaled as indicated in both panels.

main features (labeled ''a1'' and ''b'') are observed in the edge and pre-edge region, while a smaller shoulder (labeled ''a2'') is only observed at the L_3 edge. 170 and 150 K XMCD curves are very similar at both edges, indicating the magnetic saturation of the sample in this range of temperature, above T_{SRT} and well below $T_c \approx 600$ K. The XMCD spectra recorded at 150, 130, and 110 K present a noticeable enhancement coincident with T_{SRT}. Below 110 K, XMCD remains again almost independent of temperature, showing no differences between 110 and 50 K. These experimental results reflect the sensibility of the technique to the SRT occurring below 135 K. However, the interpretation of the observed thermal variations is not simple: the spectra recorded at different temperatures do not scale, as it should be the case if the whole signal would have a single dipolar (E1) origin and the only differences would be originated by $\theta_{Nd}(T)$. This is more evident at the L_2 edge, where the a1 feature is only observed below T_{SRT}. It has been theoretically pointed out[1,5] and experimentally confirmed[6] that the pre-edge features in $L_{2,3}$ dichroic spectra in rare earth ions have its origin in quadrupolar (E2) $2p \rightarrow 4f$ transitions.

XRMS is the scattering counterpart of XMCD.[7] It allows to discriminate the multipolar origin of the observed magnetic signals by studying different Bragg reflections, as dipolar and quadrupolar contributions have different angular dependence. We performed room-temperature XRMS on $Nd_2Fe_{14}B$ on several $(hh0)$ reflections at the $L_{2,3}$ edges of Nd. $(hh0)$ Bragg reflections were selected because the two nonequivalent crystallographic sites occupied by Nd ions, $4f$ and $4g$, contribute very differently to the structure factor for different h values. This fact, although it is not the objective of the present study, allow to deconvolute the resonant magnetic signal created by Nd ions occupying $4f$ and $4g$ sites.

The experimental results are shown in Fig. 2. Their spectral shape reflects roughly that of XMCD and, within the experimental errors, the same features are present at both edges (a1 feature is visible even at room temperature in (220) and (330) reflections at the L_2 edge). Full lines in Fig. 2 are the results of a fitting procedure based on the standard interpretation of XRMS[7] by means of a regularization technique analysis. A proper fitting of the whole data set was only possible by allowing for a E2 origin for a1 and a2 features, with an intensity which at the L_3 edge is comparable to that of the E1 one (b and higher energy features).

Standard absorption measurements at the $L_{2,3}$ edges of rare-earth ions cannot separate the two E1 and E2 excitation channels due to the $2p$ core-hole lifetime broadening. However, it has been shown that such a separation can be achieved by means of resonant inelastic x-ray scattering (RIXS) experiments.[8] In Nd, this can be realized by studying the resonance behavior of the $4d^9 4f^4 5d^0$ and the $4d^9 4f^3 5d^1$ final state multiplets as the incident photon energy is tuned through the $2p^5 4f^4 5d^0$ and $2p^5 4f^3 5d^1$ intermediate state excitation energies, monitoring the $4d_{5/2,3/2} \rightarrow 2p_{3/2}$ radiative decay channel $L\beta_{2,15}$ of Nd. In Fig. 3 (left panel), we present as a function of the energy transfer, ΔE, four representative RIXS spectra obtained at different fixed incident energies, E_i, (indicated in the figure) in the vicinity of the Nd L_3 edge. The spectrum recorded at $E_i = 6210$ eV $\approx E_{L3}$ corresponds to the largest incident energy at which the maximum of the central feature, labeled ''B,'' remains at $\Delta E \approx 121.6$ eV, indicating that the photoelectron has been excited to a $5d$ localized intermediate state without acquiring extra kinetic energy. At higher incident energies (upper curve), this feature moves towards higher ΔE as the photoelectron acquires extra kinetic energy when promoted to the $5d$ band. The two lower spectra were recorded with E_i in the pre-edge region. Two extra channels, labeled ''A1'' and ''A2'' appear as distinct shoulders in the RIXS spectra at $\Delta E \approx 115.5$ and 118.5 eV. Previous experimental results[8] and theoretical calculations[9] allow an unambiguous assignment of features A1, A2, and B. Feature B is assigned to the $4d^9 4f^3 5d^1$ final state multiplet, resonantly enhanced at the $2p^5 4f^3 5d^1$ intermediate state excitation energies, corresponding to the strong dipolar $2p \rightarrow 5d$ channel. Features A1 and A2 are ascribed to the $4d^9 4f^4 5d^0$ final state multiplets which are resonantly enhanced at the $2p^5 4f^4 5d^0$ intermediate state excitation energies, corresponding to the weak quadrupolar $2p \rightarrow 4f$ excitation channel. Features A1 and A2 are observed at lower ΔE values than feature B, i.e., at smaller intermediate state excitation energies. This is consistent with the strength of the Coulomb interaction between the pro-

moted electron and the $4d$ core hole resulting in a $4d^9 4f^4 5d^0$ final state more strongly bound than the $4d^9 4f^3 5d^1$ or $4d^9 4f^3 5d^1 \epsilon^*$ states.

To directly compare the inelastic scattering spectra with the XMCD, the evolution of the peak intensities of features A1, A2, and B is monitored by scanning the incident and scattered photon energy together, thus keeping ΔE constant and fixed to the values corresponding to the excitation energies of features A1, A2, and B, respectively. These constant-final-state (CFS) spectra are reported in Fig. 3 (right panel, thin line) together with the corresponding L_3 edge XMCD (thick line) measured on the same sample.

It is evident that features A1, A2, and B correspond to three different resonances, reaching their maximum intensity at different incident photon energies and that their correspondence with the XMCD features below and at the edge is rather evident. The energy position around which the dipolar B resonance is centered corresponds to the strongest feature in the XMCD spectra. This observation is in agreement with the commonly accepted interpretation of the XMCD signal at the absorption threshold. More importantly, A1 and A2 features resonate at two different energies, in coincidence with the a1-a2 structure in the Nd L_3 XMCD.

Once the origin of a1, a2, and b features of the XMCD spectra at the L_3 edge has been determined, we can properly treat the temperature variation of the dichroic signals, obtaining information about $\theta_{\mathrm{Nd}}(T)$. Although the strong differences in the relative E2/E1 intensity between the two absorption edges remain to be fully explained, there have been theoretical efforts[10] which qualitatively describe the observation, predicting an up-to-now never observed quadrupolar contribution to the XMCD at the L_2 edge of rare-earth ions. It is well known[11] that the intensity of a dichroic E1 contribution depends linearly on $(W_{1,1}-W_{1,-1})\cos\alpha$, while a E2 one is proportional to $((W_{2,1}-W_{2,-1})\cos 2\alpha+(W_{2,2}-W_{2,-2})\sin^2\alpha)\cos\alpha$, where $W_{L,M}$ are the matrix elements the 2^L pole transitions. Given the order of magnitude of the involved transition energies, $W_{L,M}$ will be treated as temperature independent in the range of interest of our study. By integration of the dichroic intensities, the $W_{L,M}$'s remain in the equations as constant factors. We have studied the temperature dependence of the E2/E1 intensity ratio at both edges. The temperature dependence of XMCD through $\mu_{\mathrm{Nd}}(T)$ is overcome by studying the ratio between two dichroic signals which depend on the same way on $\mu_{\mathrm{Nd}}(T)$. The experimental ratio values obtained at both edges are shown in Fig. 4. Furthermore, we have fitted the temperature dependence of the E2/E1 ratio to the theoretical angular dependence calculated by using the $\theta_{\mathrm{SR}}^{\mathrm{Nd}}(T)$ values corresponding to the strongly noncollinear arrangement in the low-temperature phase conjectured by Onoedera[2] from ^{57}Fe Mössbauer spectroscopy data. The remarkable agreement of the fit to the experimental E2/E1 ratio strongly supports Onoedera's prediction, with an average value of $\theta_{\mathrm{Nd}}\approx 57°$ to compare with $\theta_{\mathrm{Fe}}\approx 27°$ at the lowest temperatures. The observed angular behavior of E2/E1 at the L_2 edge (coincident with that from L_3) is, to the authors knowledge, the first experimental evidence of a quadrupolar contribution to the dichroism of a rare-earth ion at the L_2 edge.

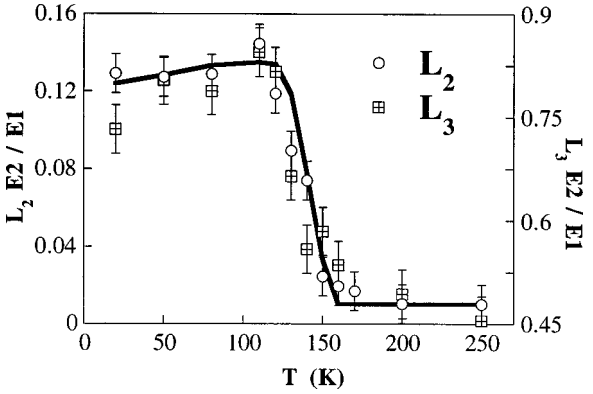

FIG. 4. Temperature dependence of the E2/E1 ratio of the XMCD spectra at the L_2 (open symbols) and L_3 (crossed squares) absorption edges. The thick line corresponds to the expected behaviour for the predicted noncollinear configuration between Fe and Nd ions in Ref. 2 for a dipolar b and quadrupolar a1 and a2 features.

In summary, our combined XMCD, XRMS, and RIXS study at the Nd $L_{2,3}$ edges in the $Nd_2Fe_{14}B$ has allowed to separately observe the E1 and E2 absorption channels, evidencing the E2 origin of the magnetic pre-edge features at both edges in XMCD and XRMS and showing how this different spectroscopic origin provides new information on the magnetic properties of materials.

This work has been partly financed by Spanish CICYT, project MAT96/448. XMCD and XRMS experiments were performed at ID12A and BM32 beamlines at the ESRF, respectively. RIXS experiments were performed at X21 at NSLS. The authors highly acknowledge the staff of both facilities for the kind support received.

[1] P. Carra and M. Altarelli, Phys. Rev. Lett. **64**, 1286 (1990).
[2] H. Onoedera, A. Fujita, H. Yamamoto, M. Sagawa, and Y. Matsuura, J. Magn. Magn. Mater. **68**, 6 (1987); **68**, 15 (1987).
[3] A. Koizumi, K. Namikawa, H. Maruyama, K. Mori, and H. Yamazaki, Jpn. J. Appl. Phys., Part 1 **32**, 332 (1993).
[4] J. F. Herbst, Rev. Mod. Phys. **63**, 819 (1991), and references therein.
[5] X. Wang, T. C. Leung, B. N. Harmon, and P. Carra, Phys. Rev. B **47**, 9087 (1993).
[6] J. C. Lang, G. Srajer, C. Detlefs, A. I. Goldman, H. König, X. Wang, B. N. Harmon, and R. W. McCallum, Phys. Rev. Lett. **74**, 4935 (1995).
[7] J. P. Hannon, G. T. Trammell, M. Blume, and D. Gibbs, Phys. Rev. Lett. **10**, 1245 (1988).
[8] M. Krisch, C. C. Kao, F. Sette, W. A. Caliebe, K. Hämäläinen, and J. B. Hastings, Phys. Rev. Lett. **74**, 4931 (1995).
[9] M. van Veenendaal and R. Benoist, Phys. Rev. B (in press).
[10] M. van Veenendaal, J. B. Goedkoop, and B. T. Thole, Phys. Rev. Lett. **78**, 1162 (1997).
[11] P. Carra, H. König, B. T. Thole, and M. Altarelli, Physica B **192**, 182 (1993).